Supporting Information for

Engineering pore structure in phenolic resin derived hard carbon via CO_2 assisted carbonization for enhanced sodium storage

Wei Wang, Binyuan Zhang, Hairu Wang, Rui Ma, Lili Ai, Mengjiao Xu, Changyu Leng, Qingtao Ma, Dianzeng Jia, Nannan Guo*, Luxiang Wang*

State Key Laboratory of Chemistry and Utilization of Carbon Based Energy Resources, College of Chemistry, Xinjiang University, Urumqi, 830017, P.R. China

Material Characterization

The crystal structure of the material was analyzed by X-ray diffraction (XRD; D8-Advance, Bruker, Germany). Surface morphology of the material was examined using scanning electron microscopy (SEM; S-4800, Hitachi, Japan). The internal microstructure was observed via transmission electron microscopy (TEM; JEM-2100F, JEOL, Japan). Raman spectroscopy (HR Evolution, HORIBA, France) was used to test defect density and graphitization degree. Chemical composition and elemental valence states were characterized by X-ray photoelectron spectroscopy (XPS; ESCALAB 250, Thermo Scientific, USA). The specific surface area and pore size distribution were determined using a fully automated surface area and porosity analyzer (ASAP 2460, Micromeritics, USA) via gas adsorption-desorption measurements. The true density of the samples was measured with a gas pycnometer (AccuPyc II 1340, Micromeritics, USA).

* Corresponding author: E-mail: guonan067@163.com (N. Guo); wangluxiangxju@163.com (L. Wang)

Chemicals and Materials

3-aminophenol, formaldehyde, N-methyl-2-pyrrolidone (NMP) and sodium pieces from Shanghai Aladdin Biochemical Technology Co., Ltd.; cetyltrimethylammonium bromide from Beijing Innochem Science & Technology Co., Ltd.; absolute ethanol and phenolphthalein from Tianjin Guangfu Fine Chemical Research Institute and Tianjin Fuchen Chemical Reagent Factory, respectively; sodium hexafluorophosphate electrolyte (DME), sodium carboxymethyl cellulose (CMC-Na) binder, and conductive agent (ECP) from Duoduo Chemical Technology Co., Ltd.; glass fiber separator from Kelude New Material Co., Ltd.; and deionized water from Xinjiang University.

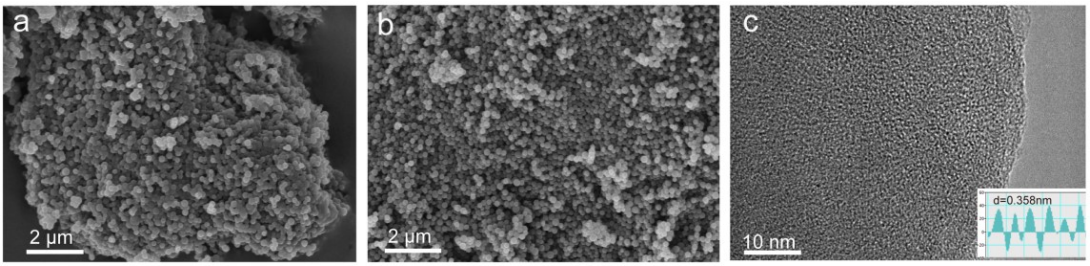

Fig. S1. (a, b) SEM images of SPC and SPCC; (C)TEM images of SPC

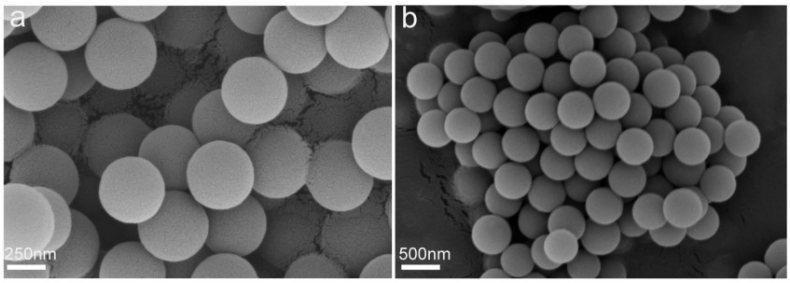

Fig. S2. (a, b) SEM images of SP

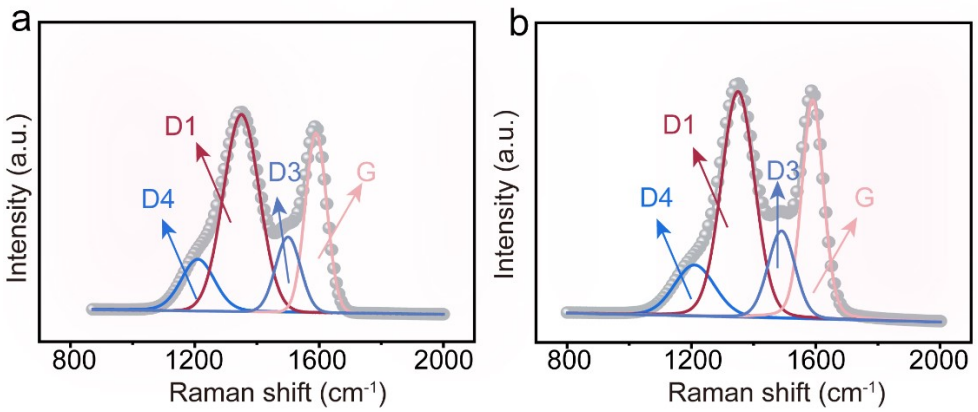

Fig. S3. Peak fitting of the Raman spectra: (a) SPC and (b) SPCC.

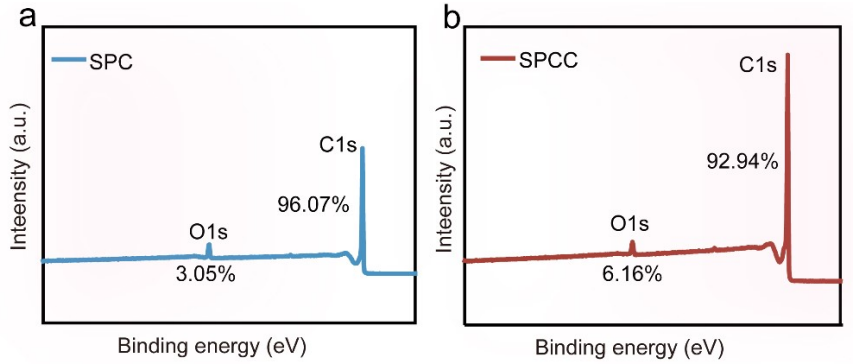

Fig. S4. XPS spectra of (a) SPC; and (b) SPCC

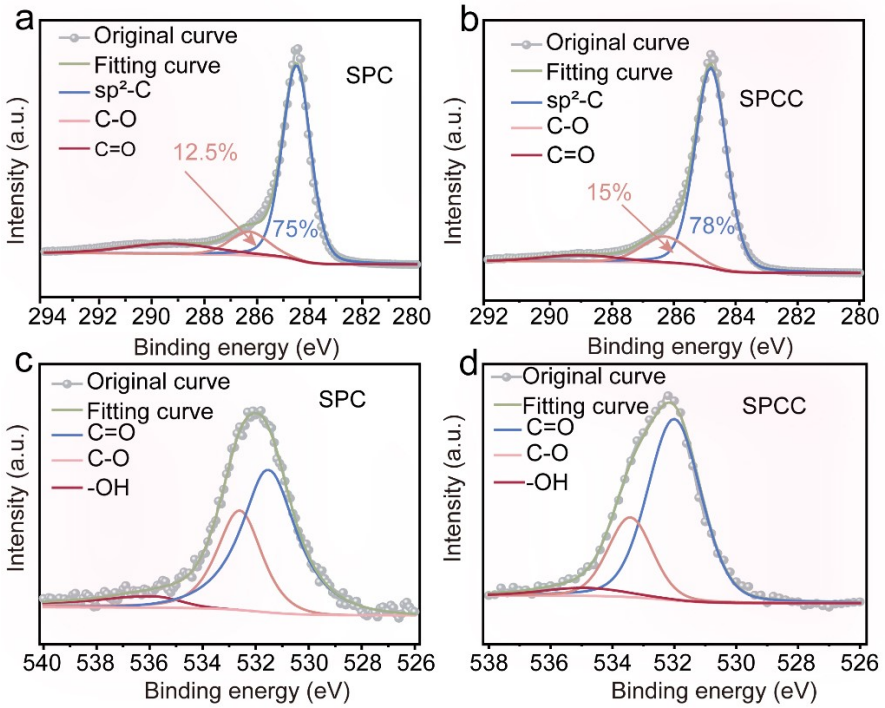

Fig. S5. (a, b) High-resolution spectra of the C1s; (c, d) High-resolution spectra of the O1s.

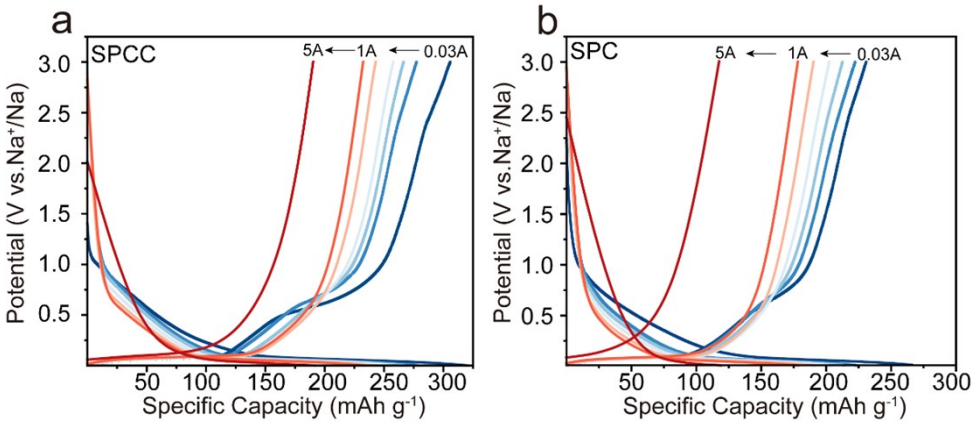

Fig. S6. The discharge-charge curves of SPCC and SPC at different current densities from 30 mA g^{-1} to 5A g^{-1}.

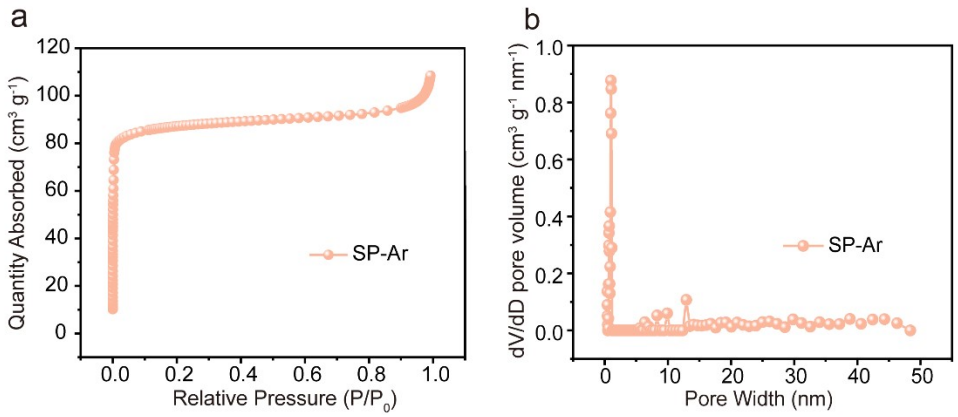

Fig S7. (a) Nitrogen adsorption–desorption isotherms and (b) pore size distribution of SP-Ar.

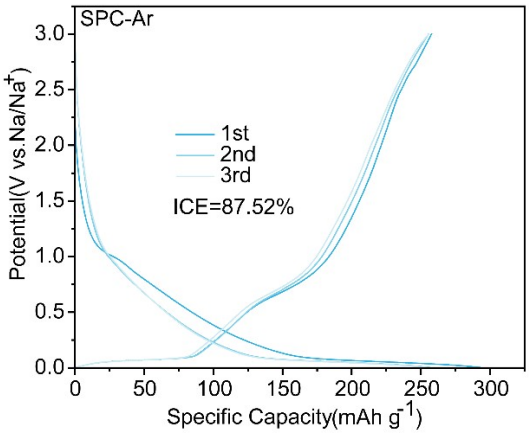

Fig S8. The first three cycles at 0.03 A g^{-1} for the SPC-Ar electrode.

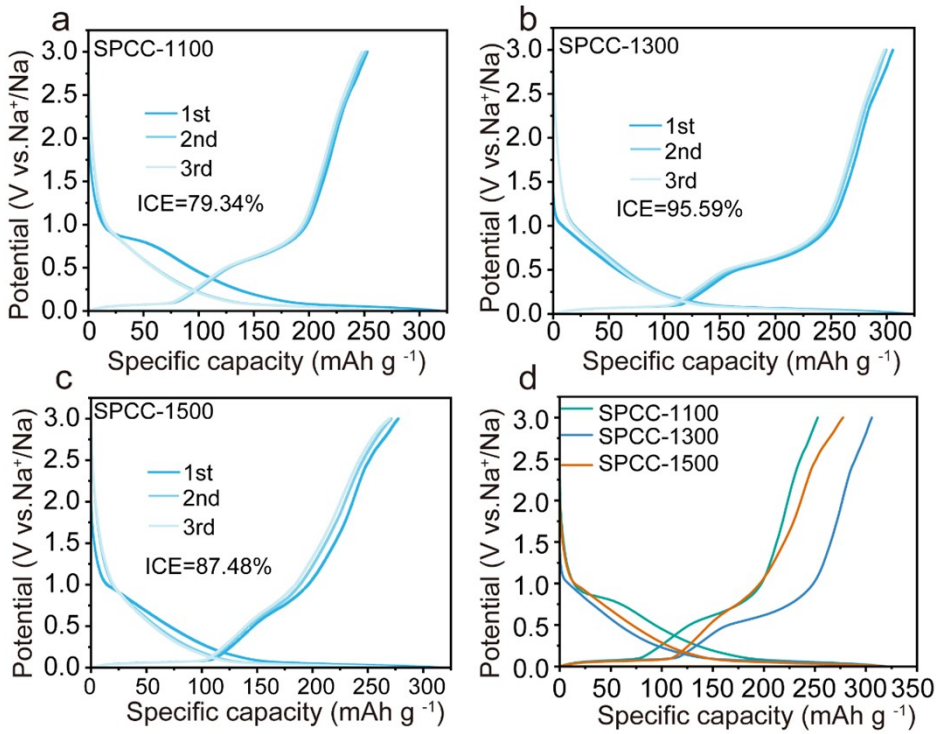

Fig. S9. GCD curves of different samples: (a) SPCC-1100; (b) SPCC-1300; (c) SPCC-1500; (d) Comparison of first-cycle GCD curves of SPCC-1100; SPCC-1300℃; and SPCC-1500

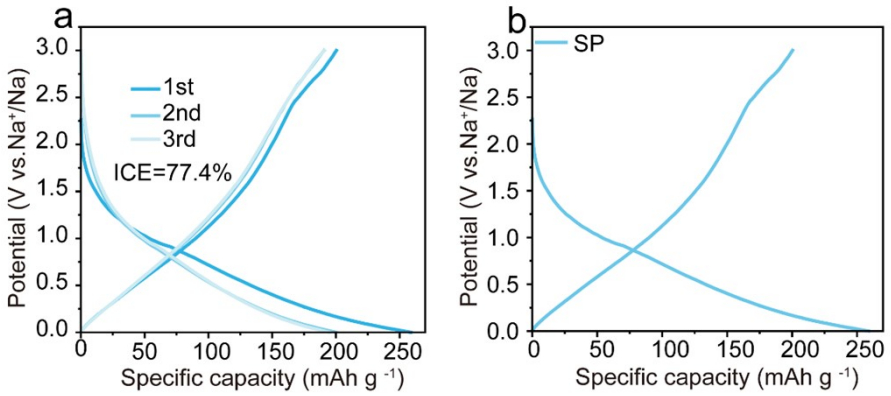

Fig. S10. The GCD curve and first three cycles at 0.03 A g^{-1} of SP

The optimal carbonization temperature for hard carbon generally ranges from 1000 °C to 1600 °C [1, 2]. In this study, a comparison of the galvanostatic charge-discharge (GCD) curves of samples prepared at three different temperatures revealed that SPCC-1300 exhibited a higher reversible capacity (305.8 mAh g^{-1}) and initial coulombic efficiency (95.6%) than SPCC-1100 (253.9 mAh g^{-1}, 81.29%) and SPCC-1500 (277.6 mAh g^{-1}, 87.48%). Lower carbonization temperatures result in underdeveloped carbon layers, which allows solvent molecules to penetrate the particles through pores, causing capacity loss. In contrast, excessive carbonization promotes the orderly stacking of carbon layers, resembling graphitization, which reduces the interlayer spacing and hinders sodium ion diffusion. Therefore, the ideal carbonization temperature for phenolic resin-derived hard carbon materials is 1300 °C [3-5] (Fig. S7). In addition, the SP (only CO_2-etched) exhibited a very low plateau capacity, likely due to its extensive open porosity from etching. This porosity facilitates the surface adsorption that is primarily responsible for the sloping region in the GCD curves. [6-8] (Fig. S8).

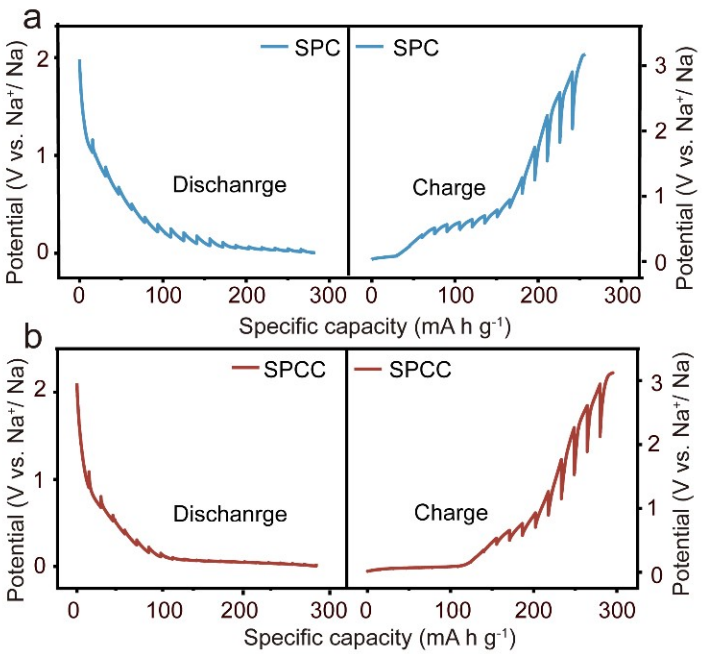

Fig. S11. GITT curves in discharge and charge, (a) SPC, (b) SPCC

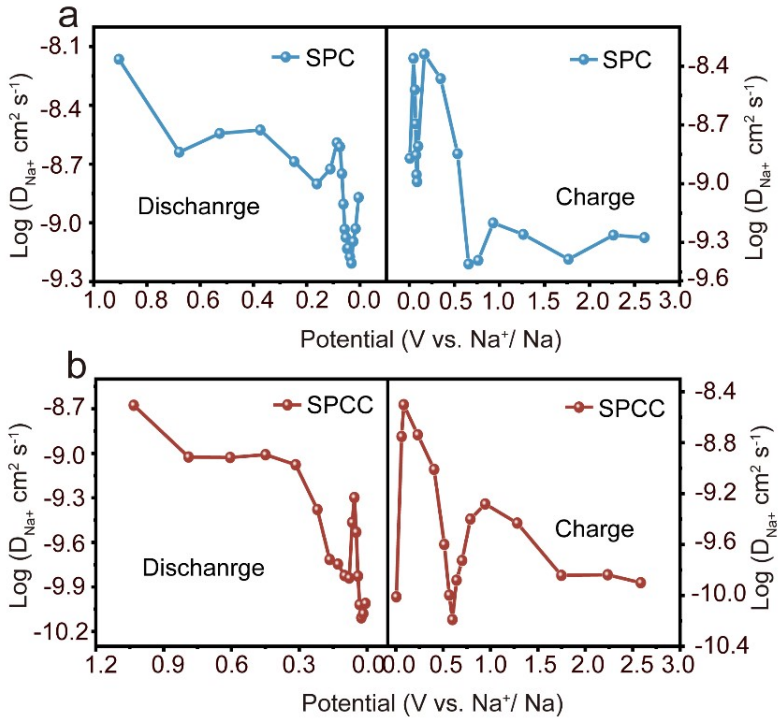

Fig. S12. diffusion coefficients for sodium ions estimated from GITT curves: (a) SPC, (b) SPCC

Table S1. True density, pore volume, pore size, and specific surface area of the samples

Samples	True density ($g\ cm^{-3}$)	Closed pore volume ($cm^3\ g^{-1}$)	Closed pore size (nm)	S_{BET} ($m^2\ g^{-1}$)
SPC	1.92	0.078	1.05	90.02
SPCC	1.78	0.119	2.10	6.58

Table S2. Performance comparison of SIB full cells reported in the literature.

Sample material	Working voltage(V)	Current density (A g^{-1})	Specific Capacity (mAh g^{-1})	Reference
NVP/HC	Average 3.35	0.05	236.7	[9]
NVP/HC	2-4	0.05	287.7	[10]
NVP/HC	Average 3.28	0.02	229.3	[11]
NVP/HC	Average 3.3	0.05	210.7	[12]
NVP/HC	2.3-3.8	0.025	231	[13]
NVP/HC	Average 2.9	0.03	243.8	[14]
NVP/HC	1.7-3.9	0.05	260.2	This work

References

1 G. L. Zhang; H. Gao; D. Y. Zhang; J. Xiao; L. M. Sun; J. Y. Li; C. C. Li; Y. W. Sun; X. Y. Yuan; P. Huang; Y. Xu; X. Guo; Y. F. Zhao; Y. Wang; Y. Xiao; G. X. Wang; H. Liu, Transformative Catalytic Carbon Conversion Enabling Superior Graphitization and Nanopore Engineering in Hard Carbon Anodes for Sodium-Ion Batteries. *Carbon Energy* (**2025**), *7* (6), e713.

2 W. J. Zhang; Y. X. Du; Y. Q. Qiu; C. Li; I. Razanau; A. Kaisha; F. Xu; H. Q. Wang, Closed-Pore Engineering in Hard Carbon for Sodium Ion Storage: Advances, Challenges and Future Horizons. *Adv. Energy Mater.* (**2025**), e03884.

3 L. Zhou; Y. P. Cui; P. C. Niu; L. N. Ge; R. M. Zheng; S. H. Liang; W. Xing, Biomass-derived hard carbon material for high-capacity sodium-ion battery anode through structure regulation. *Carbon* (**2025**), *231*, 119733.

4 W. L. Zhang; Z. Jiang; W. B. Jian; L. Zhong; Y. Y. Chen; X. H. Zu; Q. Y. Liu; X. Q. Qiu, Structural Reconstruction of Lignocellulose toward Hard Carbons for Optimized Sodium-Ion Storage. *ACS Appl. Mater. Interfaces* (**2025**), *17* (31), 44639-44656.

5 J. Q. Zheng; C. H. Guan; H. X. Li; D. J. Wang; Y. Q. Lai; S. M. Li; J. Li; Z. Zhang, Unveiling the Microscopic Origin of Irreversible Capacity Loss of Hard Carbon for Sodium-Ion Batteries. *Adv. Energy Mater.* (**2024**), *14* (15), 2303584.

6 G. Huang; H. Zhang; F. Gao; D. Y. Zhang; Z. Q. Zhang; Y. Liu; Z. T. Shang; C. Q. Gao; L. B. Luo; M. Terrones; Y. Q. Wang, Overview of hard carbon anode for sodium-ion batteries: Influencing factors and strategies to extend slope and plateau regions. *Carbon* (**2024**), *228*, 119354.

7 W. Zhao; S. Zhang; H. H. Lai; W. X. He; B. K. Yap; U. Feleni; X. W. Peng; J. L. Cui; L. X. Zhong, A Dual-Phase Pore Engineering Strategy to Enhance Low-Voltage Plateau Capacity of Hard Carbon for Sodium-Ion Batteries. *Carbon Energy* (**2025**), e70047.

8 R. Ma; Y. X. Chen; Q. Li; B. Y. Zhang; F. F. Chen; C. Y. Leng; D. Z. Jia; N. N. Guo; L. X. Wang, Oxygen-driven closing pore formation in coal-based hard carbon for low-voltage rapid sodium storage. *Chem. Eng. J.* (**2024**), *493*, 152389.

9 W. C. Ren; L. Yang; X. Y. Wang; C. L. Qiu; J. Shi; J. W. Chen; W. Q. Tian; M. H. Huang; H. L. Wang, Synergistic CO2 etching and carbonization induces closed-pore structures for plateau-dominant sodium storage. *Nano Res.* (**2025**), *18* (11), 94908108.

10 S. Guo; Y. M. Chen; L. P. Tong; Y. Cao; H. Jiao; Z. Long; X. Q. Qiu, Biomass hard carbon of high initial coulombic efficiency for sodium-ion batteries: Preparation and application. *Electrochim. Acta* (**2022**), *410*, 140017.

11 M. Wang; F. Cheng; F. Liu; Y. Chen; Z. Ju; J. Jiang; Y. Xing; X. Gui, Gas-driven pore engineering: From micropore generation to closed-pore structure modulation in coal-derived hard carbon for sodium-ion batteries. *Carbon* (**2026**), *248*, 121171.

12 Q. Y. Zhang; F. Yuan; Q. J. Sun; Q. J. Wang; Z. J. Li; D. Zhang; H. L.

Sun; B. Wang, Reasonable regulation of carbon layers and micropores to promote the extreme capacity of hard carbons for sodium-ion batteries. *Appl. Surf. Sci.* (**2024)**, *664*, 160277.

13 R. Samanta; S. Roy; S. Barman, Sulfur and Nitrogen Codoped Hard Carbon with Expanded Interlayer Distance as an Effective Anode Material for Sodium-Ion Batteries. *Energy Fuels* (**2024)**, *38* (20), 19867-19877.

14 L. Y. Pei; L. T. Yang; H. L. Cao; P. Z. Liu; M. Zhao; B. S. Xu; J. J. Guo, Cost-effective and renewable paper derived hard carbon microfibers as superior anode for sodium-ion batteries. *Electrochim. Acta* (**2020)**, *364*, 137313.